


RESEARCH

Open Access



Effects of transcranial ultrasound stimulation pulsed at 40 Hz on A β plaques and brain rhythms in 5 \times FAD mice

Mincheol Park^{1†}, Gia Minh Hoang^{1†}, Thien Nguyen¹, Eunkyung Lee¹, Hyun Jin Jung², Youngshik Choe², Moon Hwan Lee³, Jae Youn Hwang³, Jae Gwan Kim^{1*} and Tae Kim^{1*} 

Abstract

Background: Alzheimer's disease (AD) is the most common cause of dementia, and is characterized by amyloid- β (A β) plaques and tauopathy. Reducing A β has been considered a major AD treatment strategy in pharmacological and non-pharmacological approaches. Impairment of gamma oscillations, which play an important role in perception and cognitive function, has been shown in mouse AD models and human patients. Recently, the therapeutic effect of gamma entrainment in AD mouse models has been reported. Given that ultrasound is an emerging neuromodulation modality, we investigated the effect of ultrasound stimulation pulsed at gamma frequency (40 Hz) in an AD mouse model.

Methods: We implanted electroencephalogram (EEG) electrodes and a piezo-ceramic disc ultrasound transducer on the skull surface of 6-month-old 5 \times FAD and wild-type control mice ($n = 12$ and 6, respectively). Six 5 \times FAD mice were treated with two-hour ultrasound stimulation at 40 Hz daily for two weeks, and the other six mice received sham treatment. Soluble and insoluble A β levels in the brain were measured by enzyme-linked immunosorbent assay. Spontaneous EEG gamma power was computed by wavelet analysis, and the brain connectivity was examined with phase-locking value and cross-frequency phase-amplitude coupling.

Results: We found that the total A β 42 levels, especially insoluble A β 42, in the treatment group decreased in pre- and infra-limbic cortex (PIL) compared to that of the sham treatment group. A reduction in the number of A β plaques was also observed in the hippocampus. There was no increase in microbleeding in the transcranial ultrasound stimulation (tUS) group. In addition, the length and number of microglial processes decreased in PIL and hippocampus. Encephalographic spontaneous gamma power was increased, and cross-frequency coupling was normalized, implying functional improvement after tUS stimulation.

Conclusion: These results suggest that the transcranial ultrasound-based gamma-band entrainment technique can be an effective therapy for AD by reducing the A β load and improving brain connectivity.

Keywords: Transcranial ultrasound stimulation, Gamma band oscillation, Amyloid- β plaques, Alzheimer's disease

Introduction

Alzheimer's disease (AD) is one of the most common neurodegenerative diseases that affects over 50 million people in the world. AD is characterized by cognitive deficits, impairment of activities of daily living, and behavioral disturbances [1], and has two major pathological

*Correspondence: jaekim@gist.ac.kr; tae-kim@gist.ac.kr

[†]Mincheol Park and Gia Minh Hoang have contributed equally to this work.

¹ Department of Biomedical Science and Engineering, Gwangju Institute of Science and Technology, Gwangju 61005, Republic of Korea
Full list of author information is available at the end of the article



hallmarks, the presence of extracellular senile plaques caused by accumulation of A β , and the intracellular neurofibrillary tangles formed from the deposition of hyper-phosphorylated tau protein [2–4]. Under normal conditions, A β plaques are degraded by microglia and astrocytes [5] and soluble A β is removed through the perivascular pathway [6, 7]. The progressive shift from soluble to insoluble brain A β pools and the impaired plaque clearance are linked to the onset and progression of AD. Although medications currently fail to prevent the aggregation of amyloid plaques in AD patients [8, 9], pharmacological and non-pharmacological treatments based on the amyloid hypothesis are still major goals in AD treatment research, especially those that aim at reducing the accumulated A β [10].

Neuronal activity with different frequencies of gamma-band (~30 to 100 Hz) oscillation occurs across multiple brain regions, where it is assumed to play an important role in perception and cognitive functions such as attention, learning, and memory encoding and retrieval [11, 12]. Gamma oscillations are produced by synaptic activity between GABAergic inhibitory interneurons and excitatory pyramidal cells [13–15]. Degeneration of spontaneous gamma synchronization and reduction in spontaneous gamma power have typically been observed in multiple AD mouse models [16–19] and human patients [20–22].

Recently, a technique based on gamma-band entrainment is emerging as a therapeutic treatment for AD. Iaccarino et al. [23] have shown that optogenetic stimulation and visual stimulation at 40 Hz decreased A β peptides and increased microglia clustering around A β plaques in the hippocampus and visual cortex in 5 \times FAD mice, respectively. In addition, Martorell et al. [24] reported that multi-sensory gamma stimulation can reduce A β plaques and improve cognitive function. However, there is currently a lack of studies regarding the therapeutic effects of gamma-band entrainment by ultrasound stimulation for AD. Transcranially delivered ultrasound can safely activate the central neural circuits and exert neuroprotective effects on dementia [25–27]. Bobola et al. [28] delivered transcranial focused ultrasound stimulation with a 2.0 MHz carrier frequency at 40 Hz pulse repetition frequency into 5 \times FAD mice for 1 h per day to one hemisphere of the brain, and found a reduction of A β plaques and activation of microglia co-localized with A β in the treated area [28]. In this study, we set out to investigate the ultrasound-based gamma-band entrainment technique as a method to reduce brain pathology in an AD mouse model.

Methods

Animals

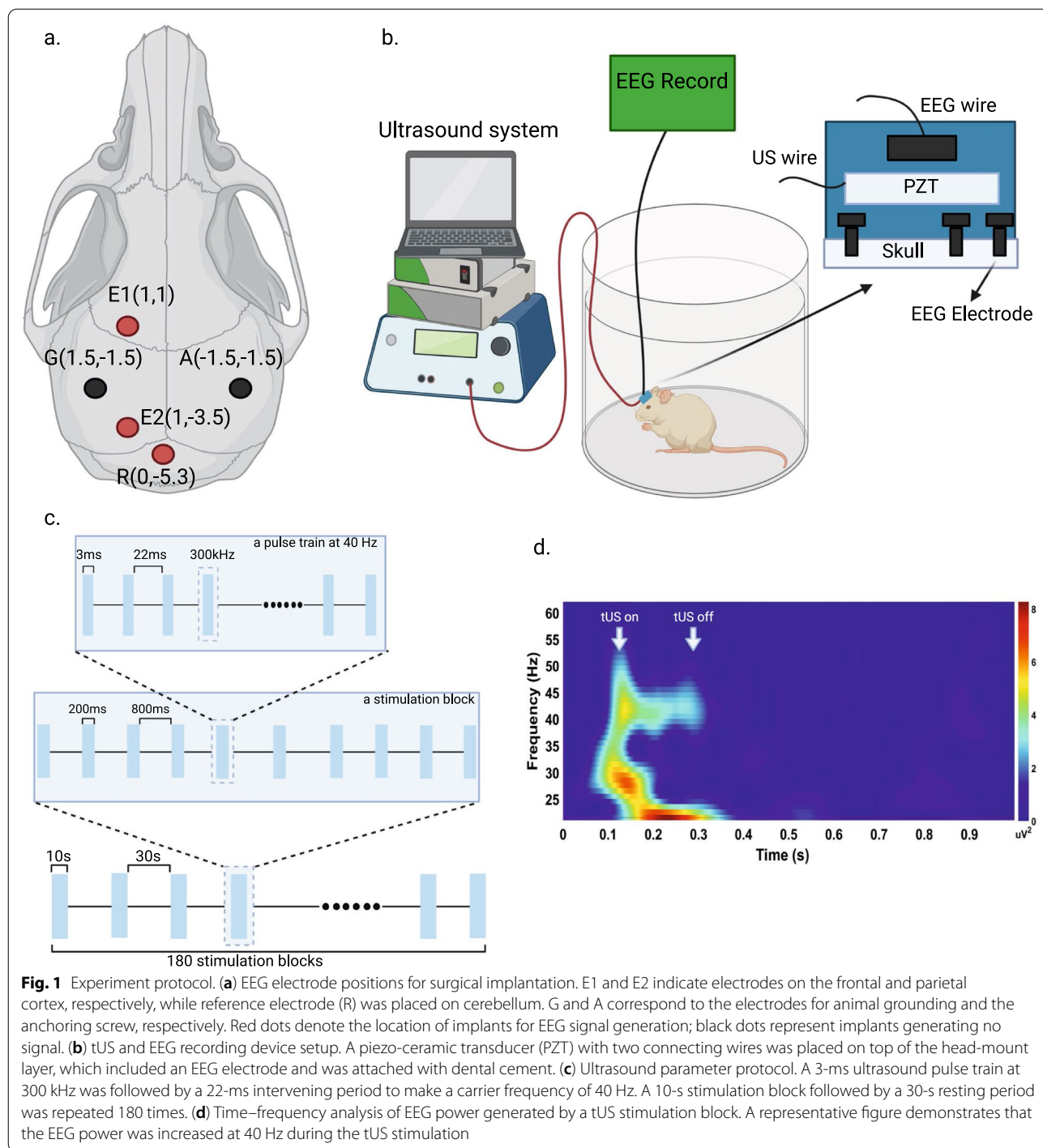
All animals were housed in a temperature- and humidity-controlled room at 20 \pm 2 °C with 55% \pm 5% humidity under a 12:12 light–dark cycle. We used 6-month-old male 5 \times FAD mice expressing human A β peptide precursor gene with Swedish, Florida, and London mutations and PS1 with mutations M146L and L286V, as at this age the 5 \times FAD mice show high A β burdens and memory impairment [29]. All animal procedures were approved by the ethics committee (GIST-2020–031), and fulfilled Association for Assessment and Accreditation of Laboratory Animal Care International guidelines.

Surgical preparation

Mice were anesthetized with 4% isoflurane and maintained with 0.5%–1.5% isoflurane in a stereotaxic frame. Ketoprofen (5 mg/kg) was injected subcutaneously before surgery as an analgesic. Electrodes for electroencephalogram (EEG) were implanted on the frontal (AP = 1.0 mm; ML = 1.0 mm) and parietal (AP = –3.5 mm; ML = 1.0 mm) areas of the skull (Fig. 1a) and connected to a premanufactured head mount (8402, Pinnacle Technology, Lawrence, KS). A piezo-ceramic disc transducer (SMD07T03R411, Steiner & Martins Inc., Davenport, FL) with two connecting wires was placed on top of the head-mount layer and combined by dental cement (Fig. 1b). We gave at least one week of recovery after surgery.

Transcranial ultrasound stimulation (tUS) experiment

Twelve male 5 \times FAD mice were assigned to the tUS treatment group (n = 6; Tg/Stim+) and the sham treatment group (n = 6; Tg/Stim-), and wild-type mice (n = 6; WT) without tUS treatment were assigned to the control group. The tUS was performed every day for two weeks. We used the piezo-ceramic disc transducer implanted to the mouse head above the EEG electrode layer. The 300 kHz ultrasonic beams pulsed at 40 Hz with 3-ms pulse width were applied transcranially. The stimulation trains of 200-ms ON and 800-ms OFF periods were repeated in stimulation blocks of 10-s ON and 30-s OFF periods (Fig. 1c). The duration of stimulation session was 2 h daily and repeated for 2 weeks. The ultrasonic beam was applied to the entire brain. The width of the ultrasound beam ranged from 5.5 to 6.0 mm. We used LabView (National Instruments Corporation, Austin, TX) to control the function generator. The signal generated by the function generator was amplified before being transferred to the piezo-ceramic disc transducer. The tUS pulsed at 40 Hz successfully induced EEG responses centered at 40 Hz, confirmed by averaging the ~1200 time–frequency plots for each mouse during 2 h of stimulation (Fig. 1d). We used ultrasound with a spatial peak



pulse average intensity (I_{SPPA}) value of 1.2 W/cm^2 and a spatial peak time average intensity (I_{SPTA}) value of 14.4 mW/cm^2 . The sonication parameters selected are considered safe and below the limits set by the US Food and Drug Administration for diagnostic ultrasound imaging ($I_{SPTA} 720 \text{ mW/cm}^2$, $I_{SPPA} 190 \text{ W/cm}^2$, Mechanical Index

1.9). The mice were sacrificed within 24 h after the last tUS treatment.

EEG recordings and data analysis

The mice were tethered to the recording system and habituated to the recording environment for 24 h before recordings (Fig. 1b). EEG of freely moving mice was

recorded with a sampling rate of 2 kHz and a low-pass filter at 100 Hz (8200-K1-SL, Pinnacle Technology, Lawrence, KS) from 00:00 to 08:00. The EEG data were analyzed offline in the customized code with Matlab and Python. Spontaneous gamma power was examined at 30–80 Hz. Briefly, the signal was filtered by a second-order Butterworth filter with a higher and a lower cut-off adjusted to 2 Hz above and 100 Hz below to remove DC noise. Spontaneous gamma power was calculated by computing the power spectral density (PSD) using Welch's method and integrating the PSD at the given frequency band using the composite Simpson's rule. The phase locking value (PLV) was calculated by applying the Hilbert transform with a determined frequency band and measuring the differences in the instantaneous phase between the frontal and parietal EEG signals. All analyses were done using a toolbox in MATLAB (Brainstorm, Mathworks). Cross-frequency phase-amplitude coupling (PAC) was calculated by the Gaussian Copula PAC method and denoising.

Enzyme-linked immunosorbent assay (ELISA)

The mice were deeply anesthetized by isoflurane and then transcardially perfused with phosphate-buffered saline (PBS). Brains were removed and dissected into two hemispheres. The right hemisphere was dissected into the brainstem, thalamus, hippocampus, cerebellum, and cortex and stored at -80°C until use. The cortical and hippocampal regions were homogenized in 20 mM Tris-HCl (pH 7.6) with 5 mM EDTA and protease inhibitor cocktail (P3100, GenDEPOT, Katy, TX). The homogenates were centrifuged at 430,000 g for 20 min at 4°C to separate the soluble and insoluble A β . The supernatants were kept at -20°C , and the pellet was resuspended in 5 mM guanidine-hydrochloride and 50 mM Tris-HCl (pH 7.6). After centrifugation at 430,000 g for 20 min at 4°C , the supernatant was collected and stored at -20°C . The total protein was quantified by BCA assay (23225, Thermo Fisher Scientific, Waltham, MA). ELISA for soluble and insoluble A β was conducted following the manufacturer's instructions (A β 42: KHB3441, A β 40: KHB3481, Thermo Fisher Scientific).

Histology

The left hemisphere was fixed in 4% paraformaldehyde (pH 7.2) in 0.1 M PBS overnight and placed in 30% sucrose in 0.1 M PBS solution until it sank at 4°C . The fixed brain tissues were cut into coronal sections (40 μm) with a cryostat (Leica Biosystems, Buffalo Grove, IL). The brain sections were rinsed three times with PBS containing 1% Triton X-100 (PBST) for 10 min each after shaking at 120 rpm at room temperature, then they were blocked in 3% normal donkey serum (D9633, Sigma Aldrich,

St. Louis, MO) in 0.5% PBST for 2 h at room temperature. The primary antibody used for microglia was rabbit anti-Iba1 (1:1000, 019-19741, Wako, Japan) and the secondary was donkey anti-rabbit IgG (1:500, A31572, Invitrogen, Waltham, MA). A β deposits were stained by 1 mM Thioflavin S (T1892, Sigma Aldrich, St Louis, MO). The section was mounted onto a silane-coated slide glass (5116-20F, Muto Pure Chemicals, Tokyo, Japan), and image acquired with a confocal microscope (LSM880NLO, Carl Zeiss, Jena, Germany). Confocal microscopic images were analyzed by the ImageJ program (National Institutes of Health, Bethesda, MD). The mouse brain areas were identified based on Paxinos and Franklin mouse brain atlas [30].

Perl's Prussian blue staining

Perl's Prussian blue staining was performed to detect hemosiderin deposits. We analyzed six brain sections at 2 mm posterior to the bregma, covering retrosplenial area, medial parietal association areas, primary somatosensory area and other cortices and hippocampus. The tissues were rinsed with TBS for 10 min at room temperature. Perl's Prussian blue staining was conducted following the manufacturer's instructions (ab150674, Abcam, Cambridge, UK). Section was mounted onto a silane-coated slide glass (5116-20F, Muto Pure Chemicals, Tokyo, Japan). Images were acquired by a slide scanner (VS200, Olympus, Tokyo, Japan) and analyzed with the ImageJ program.

Stereological quantification of A β plaques and microglia

Histological images of four serial coronal sections with 200- μm distances in PIL (AP+2.1, 1.9, 1.7 and 1.5 mm from bregma) and hippocampus (AP+1.2, 1.4, 1.6 and 1.8 mm from bregma) were obtained with confocal microscopy (FV3000RS, Olympus, Tokyo, Japan). A β plaques and microglia were quantified using an unbiased stereological dissector method by ImageJ software. The images of regions of interest were acquired using a 40 \times objective according to the atlas of Paxinos and Franklin [30]. The average thickness of mounted sections was approximately 38 μm . The optical dissector height was 10 μm , with 1- μm distances between consecutive images. In each region of interest, A β plaques and microglia were counted in a frame size of 120 μm \times 120 μm (PIL) or 200 μm \times 200 μm (hippocampus), and a grid size of 250 μm \times 250 μm (PIL) or 420 μm \times 420 μm (hippocampus).

Analysis of microglial morphology

Z-stacked images of Iba1 immunohistochemistry were projected with maximum intensity and converted to binary and skeletonized images using ImageJ. The

number of microglia was manually counted for each image. The Analyze Skeleton Plugin was used to measure microglial ramification. For each section, the total number of endpoints and the length of microglial processes were normalized to the number of microglia.

Data analysis

Statistical analyses for histological data were performed using the Prism 9 software (GraphPad Software, Inc., La Jolla, CA), and electrophysiological data were analyzed by RStudio software (RStudio, Boston, MA). Independent *t*-test or Mann–Whitney Rank Sum tests were used to compare two groups; one-way ANOVA with Tukey's *post-hoc* test was used to compare three groups. Fisher's exact test was used in the analysis of contingency table.

Results

No increase in intracerebral microbleeds after tUS stimulation

To examine the potential toxic effects of the stimulation, we quantified the hemosiderin deposits using Perls' Prussian blue staining to compare the intracerebral microbleeds (Fig. 2a). The numbers of mice with hemosiderin deposits did not differ significantly between the tUS and sham stimulation groups ($P=0.455$ by Fisher's exact test; Fig. 2b). Instead, the median number of hemosiderin deposits per brain section was lower in the Tg/Stim+ group, although there was no statistical significance (Fig. 2c).

A β loads in cortical and hippocampal regions changed after two weeks of tUS at 40 Hz

In the PIL, there was a significant decrease in total A β 42 in the Tg/Stim+ group compared to the Tg/Stim- group

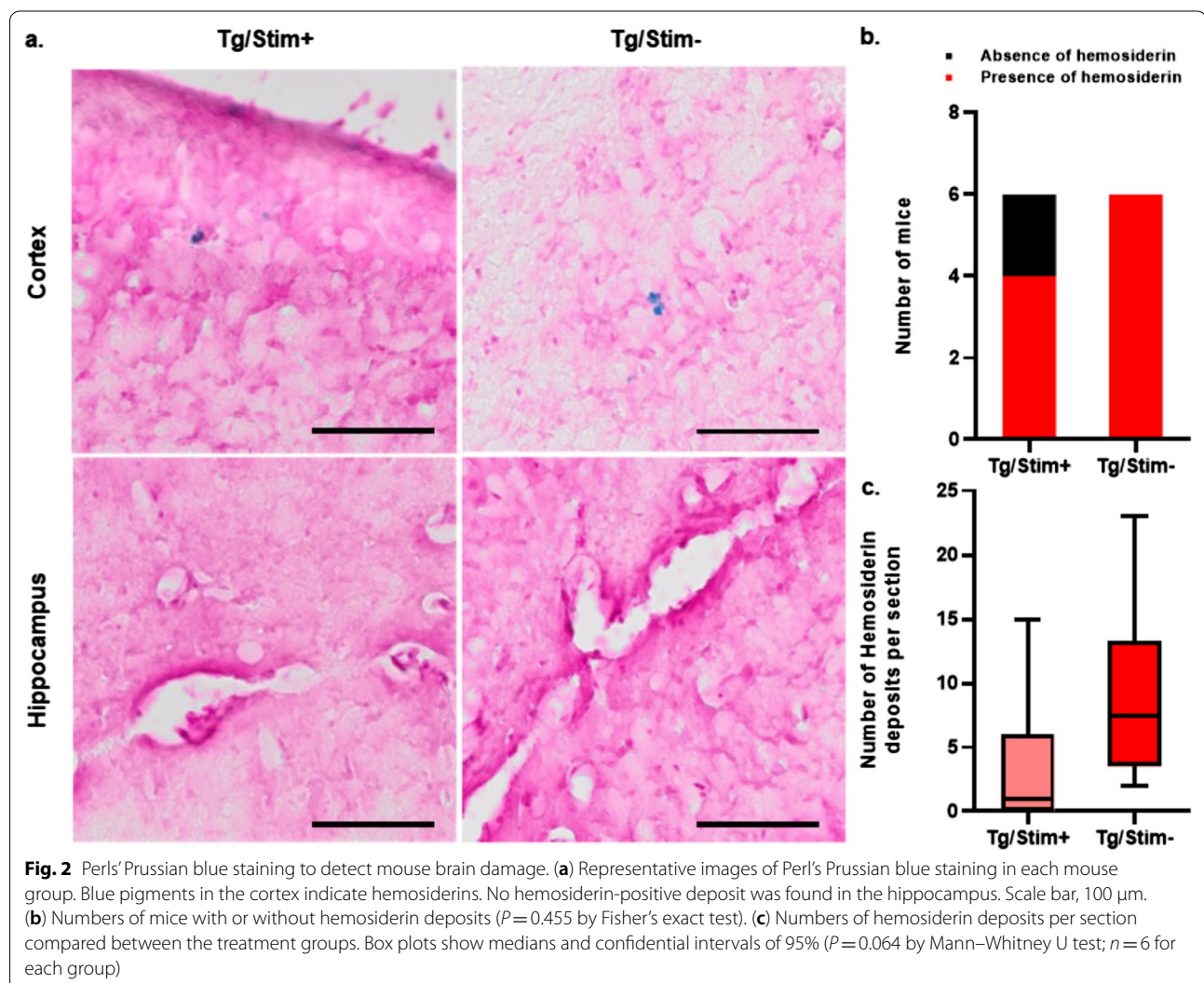
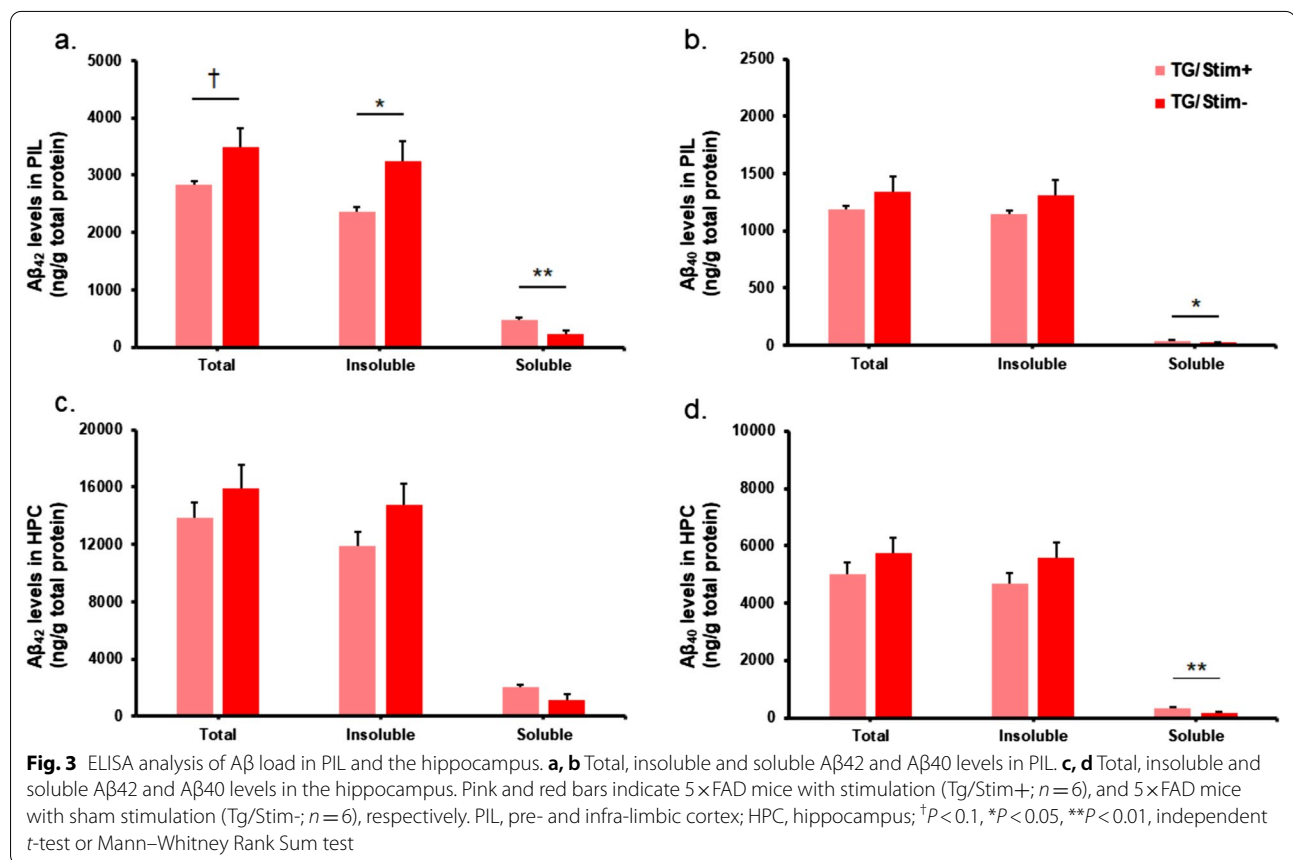


(Fig. 3a). Sub-fraction analysis showed a significant reduction of insoluble A β 42 and increase of soluble A β 42 levels in the Tg/Stim+ group compared with the Tg/Stim- group ($P < 0.05$; Fig. 3a). We also observed a decrease in total and insoluble A β 40 levels in the Tg/Stim+ group compared with the Tg/Stim- group, but the difference was not significant (Fig. 3b). In the hippocampus, A β level showed similar patterns of change, but the difference was not significant ($P > 0.05$; Fig. 3c, d). Unbiased stereological analysis showed that in the hippocampus, the estimated number of A β plaques per unit area was diminished in the Tg/Stim+ group compared to the Tg/Stim- group ($P = 0.051$; Fig. 4a, b). The Tg/Stim+ did not show significant differences in the estimated number of microglia per unit area from the Tg/Stim- group in PIL and hippocampus (Fig. 4c). To examine microglial activation, we analyzed the morphology of microglia in PIL and

hippocampus. Microglia in the Tg/Stim+ group showed a reduced number of process endpoints and decreased process length in the PIL compared to WT (Fig. 4d, e). Also, the hippocampal microglia of the Tg/Stim+ group showed a trend of decrease in the length and the number of processes compared to the Tg/Stim- group ($P = 0.086$ and 0.091 , respectively; Fig. 4d, e).

Relative spontaneous gamma power and phase-locking value in EEG changed after 2 weeks of tUS at 40 Hz

Power spectral analysis (Welch's method) was performed with a range of gamma frequencies (30–80 Hz). The gamma power was then normalized to the total power. ANOVA and *post-hoc* multiple comparisons revealed that at baseline and after 7-day stimulation, both Tg/Stim+ and Tg/Stim- groups had significantly lower



(See figure on next page.)

Fig. 4 Quantification of A β plaques and microglia and morphological analysis of microglia. **a** Representative images of microglia and A β plaque in PIL (Scale bar, 100 μ m). **b** Estimated number of A β plaques per unit area in PIL and HPC ($P = 0.051$ by two-sample *t*-test) analyzed by unbiased stereology. **c** Estimated number of microglia per unit area in PIL and HPC analyzed by unbiased stereology. **d** Average length of microglial processes per cell in PIL and HPC. **e** Average number of microglia process endpoints per cell in PIL and HPC. $* P < 0.05$, one-way ANOVA with Tukey *post-hoc* test, $n = 3$

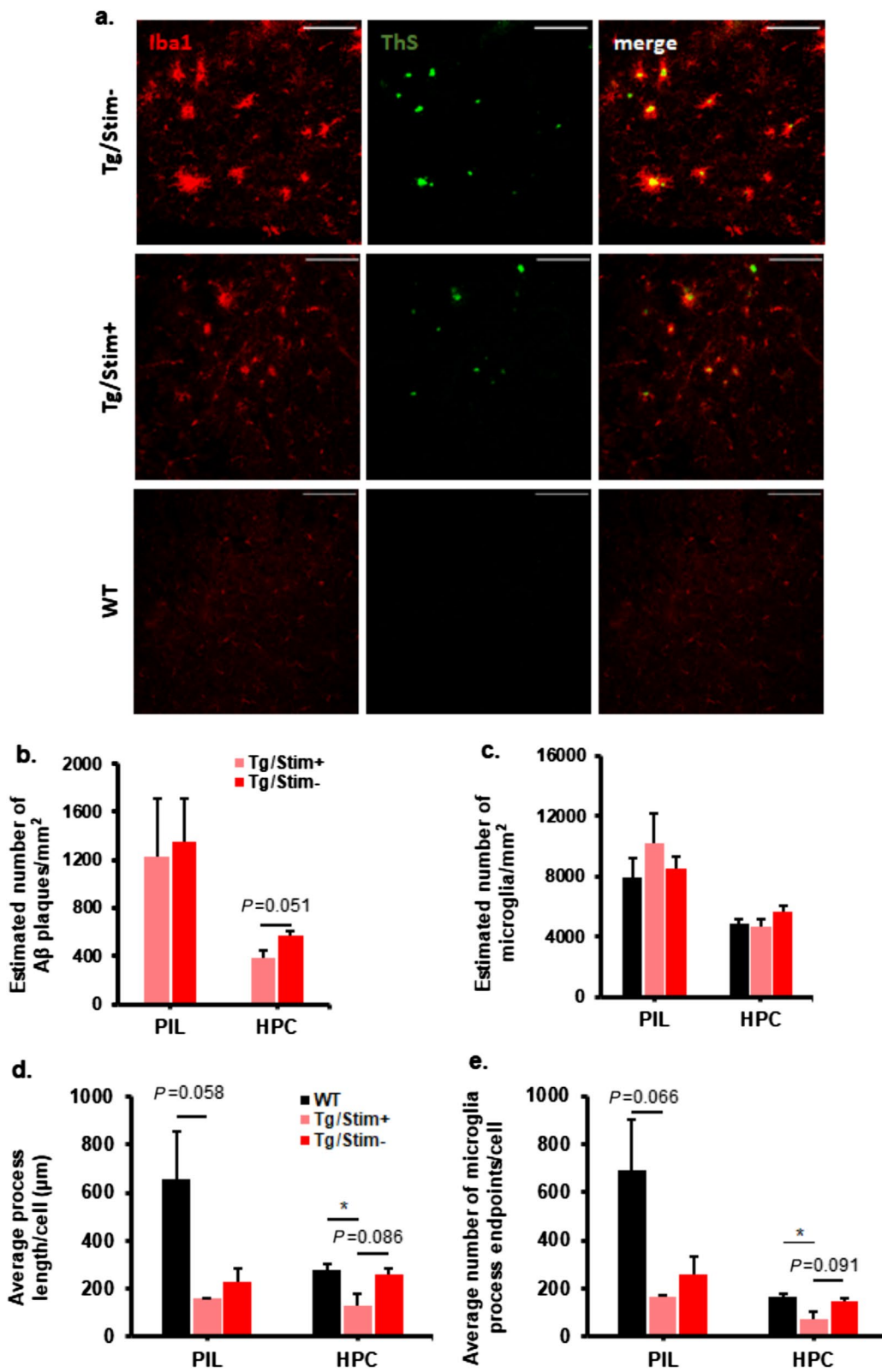
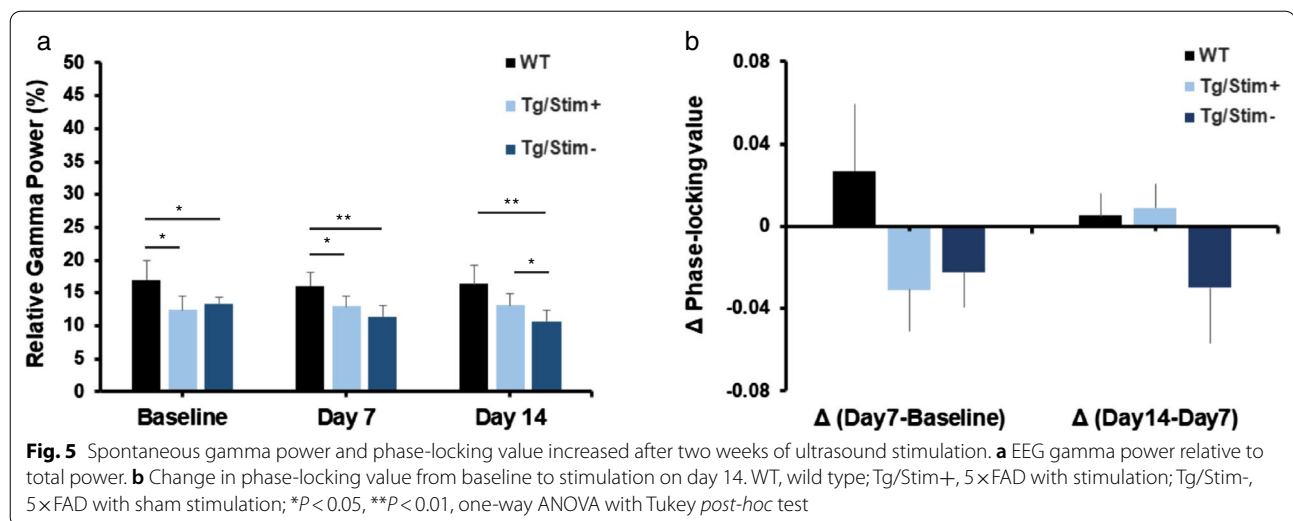


Fig. 4 (See legend on previous page.)



spontaneous gamma power than the WT mice (Fig. 5a). However, after 14-day stimulation, the spontaneous gamma power of 5×FAD mice with tUS stimulation was significantly higher than that of 5×FAD mice without tUS stimulation ($P < 0.05$), and became comparable to that of the WT mice ($P > 0.05$).

PLV was calculated at the spontaneous gamma frequency, and differences of PLV at day 7 *versus* baseline and at day 14 *versus* day 7 were calculated for each group, to investigate the change of synchronization of spontaneous gamma between frontal and parietal EEG signals. There was an increase of PLV from baseline to day 7 in the WT group, but both Tg/Stim+ and Tg/Stim- groups showed a downward trend (Fig. 5b). In addition, from day 7 to day 14, the PLVs in Tg/Stim+ and WT groups showed a trend of increase, whereas the PLV of the Tg/Stim- group remained reduced (Fig. 5b).

Cross-frequency PAC changed after 2 weeks of tUS stimulation at 40 Hz

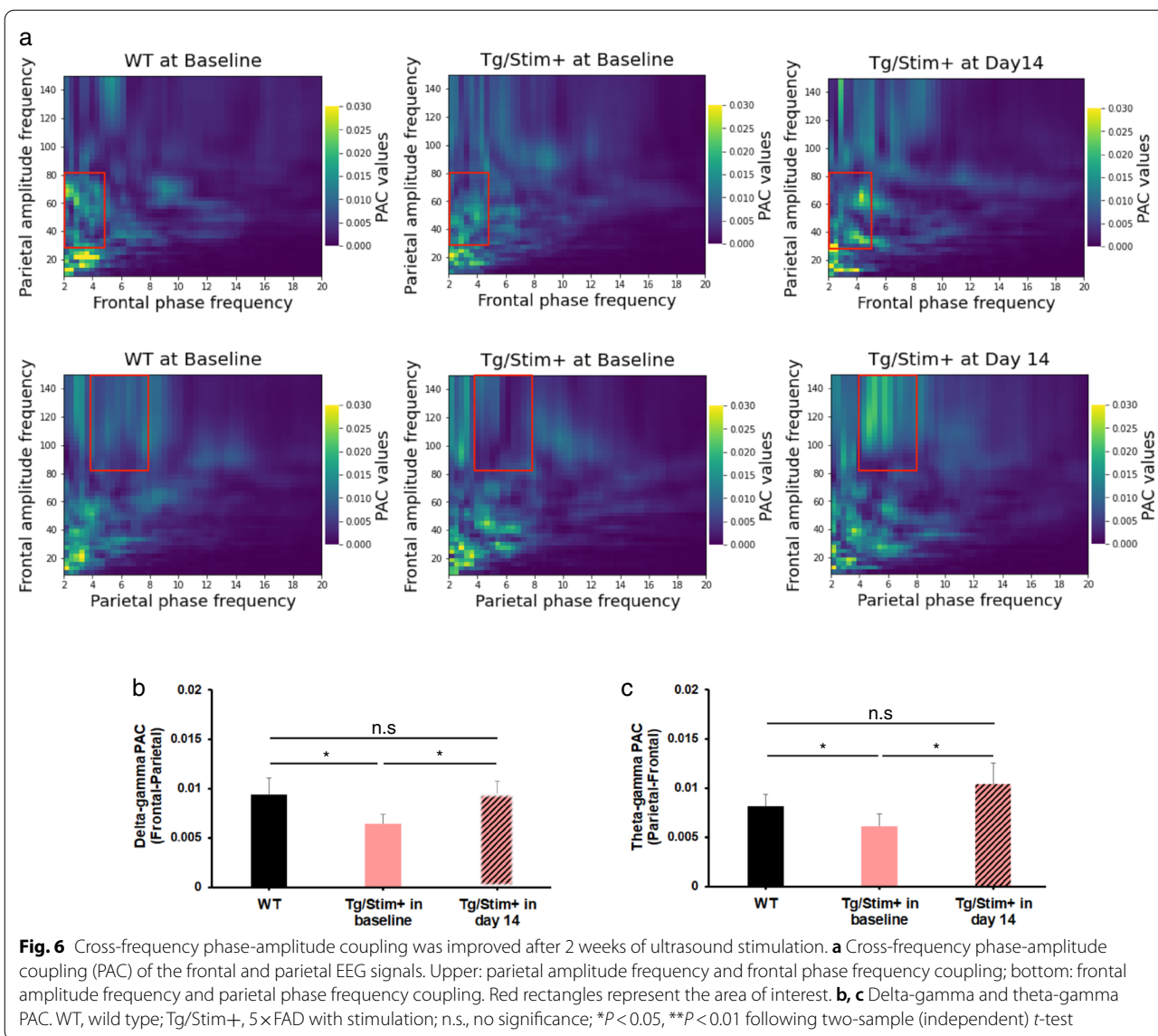
Regarding PAC, a decreased coupling of delta-phase (2–5 Hz; frontal EEG) and gamma-amplitude (30–80 Hz; parietal EEG) at baseline in Tg/Stim+ was observed compared to WT, but this coupling was improved on the last day of 14-day stimulation (Fig. 6a upper panels and 6b). The coupling of theta-phase (5–8 Hz; parietal EEG) and gamma-amplitude (80–160 Hz; frontal EEG) increased in Tg/Stim+ after 14-day stimulation compared to that at baseline (Fig. 6a lower panels and 6c). Due to the heterogeneous types of data in the three groups, we performed pairwise comparisons using the independent and paired *t*-test.

Discussion

To suggest tUS as a treatment modality, it is of utmost importance to exclude potential toxicity. In AD, cerebral amyloid angiopathy is three times more prevalent than in the general population [31]. In this study, we found no increase in microbleeds after tUS stimulation compared to the sham group, suggesting that tUS is a safe neuro-modulatory tool with the present stimulation protocol. Indeed, the energy density of our tUS stimulation was under the safety limit. Moreover, here we observed that the 14-day ultrasonic stimulation at 40 Hz gamma frequency decreased A β load in PIL and hippocampus in an animal model of AD. In addition to the molecular and histologic improvement, we found neurophysiological evidence of functional improvements, such as increased spontaneous gamma oscillations, PLV, and PAC throughout the treatment course. The novelty of our approach is to apply non-focusing ultrasound pulsed at 40 Hz, which may be an optimal stimulation modality to achieve efficacy and safety. However, the stimulation protocol must be optimized to achieve improved efficacy and safety by systematic trials with more extended stimulation periods, higher energies, and other frequencies in future studies.

Neuromodulatory effects of ultrasound stimulation

Recent studies have already shown that ultrasound stimulation can exert neuroprotective effects. Eguchi et al. [25] demonstrated that ultrasound stimulation with a pulse repetition frequency of 1 kHz could reduce A β plaque, increase cerebral blood flow, and affect endothelial nitric oxide that is considered as an important therapeutic target for AD [5]. Additionally, Huang et al. have reported that low-intensity pulsed ultrasound is effective in improving the density of dendritic spines,



altering electrophysiological properties, and increasing the expression of *N*-methyl-*D*-aspartate (NMDA) receptor 2A in the hippocampus [26]. All of these findings provide strong evidence for the beneficial effects of ultrasonic neuromodulation. Here, ultrasound stimulation with pulse repetition frequency of ~300 kHz was selected due to its higher efficacy in human and animal brain neuromodulation compared with other higher frequencies. Previous studies [32, 33] have shown that neuromodulation in vivo is more effective at frequencies less than 1 MHz, especially 300 kHz, than at 1 MHz. In addition, here the tUS stimulation pulsed at 40 Hz resulted in a strong response, similar to the auditory steady-state response to the click sounds at 40 Hz [34]. Although we focused on the impacts of gamma oscillations, effects

from other frequencies, which are beyond the scope of the current study, cannot be excluded.

Advantage and disadvantage of gamma entrainment by tUS

Gamma entrainments of neurons have been suggested as one of the promising methodologies for AD treatment. Iaccarino et al. showed that neuronal entrainment at gamma frequency by light flickering or optogenetics could reduce A β in an animal model with A β overproduction, by enhancing the phagocytic activity of microglia in the brain [23]. Subsequently, the same group showed that visual and auditory entrainment at 40 Hz could also improve A β pathology and cognitive function [24, 35]. These gamma entrainments via sensory neural systems,

such as visual and auditory pathways, have advantage of safety and thorough engagement of the implicated neural networks due to the usage of the endogenous systems, but their driving efficiency can be limited by the individuals' neural system *per se*. For example, if the sensory systems are affected by the pathological process, the effect of gamma entrainment will reduce accordingly. It is noteworthy that hearing and visual disturbances are not uncommon in the elderly. On the other hand, focused ultrasound stimulation may increase the risk of inflammatory response and tissue damage, such as intracerebral microbleeds. Therefore, a novel methodology that can enable gamma entrainment of the brain in a non-invasive and wide-ranging manner is required. We suggest that the tUS stimulation can address these problems in AD treatment with gamma entrainment.

tUS stimulation can entrain gamma band oscillations

Fast-spiking parvalbumin (PV) cells are GABAergic interneurons that account for ~40% of inhibitory interneurons and receive NMDA excitatory input from pyramidal cells [17, 36]. The regulation of fast-spiking PV interneurons through GABAergic inhibitory synaptic activity onto excitatory pyramidal cells generates and fine-tunes gamma oscillations [13–15]. Gamma oscillations in neural networks play an important role in perception and cognition, including the allocation of attention and working memory. Previous studies have shown that the gamma oscillation is reduced in AD [17, 21]. In 2012, Verrett et al. reported recovery of the gamma activity by increasing Nav1.1 expression in PV cells followed by the reduction of network hyper-synchronization and cognitive function loss in the AD animal model [17]. In our study, we observed that tUS at 40 Hz could entrain the gamma-band oscillations. The relative gamma power increased significantly after 2 weeks of ultrasound stimulation, whereas that of the non-treatment group (Tg/Stim-) remained significantly decreased compared to WT.

We speculate that the improvement of spontaneous gamma may be related to the reduction of insoluble A β . Indeed, A β can trigger Th1 cells to release IFN- γ [37], resulting in disturbed neuronal network oscillations via microglial activation and increased nitric oxide [38]. Furthermore, we observed morphological changes of microglia that imply microglial activation. Recently, it has been reported that gamma entrainment by optogenetics or visual stimulation enhances the phagocytic activity of microglia [23]. Depending on the polarization, microglia can be either pathogenic or therapeutic. The activated microglia in our experiment might also signify a microglial phenotype switch from pro-inflammatory M1 to anti-inflammatory M2 subtype. Unfortunately,

our histological marker Iba1 could not distinguish the subtypes of microglia. Considering that the M2 microglia have increased phagocytic activity, we speculate that tUS may reduce insoluble A β by phagocytic activity of M2 microglia. In addition, since GABA tonically released from reactive astrocytes might play a role in memory dysfunction [39] and, potentially, impaired gamma oscillations, we also postulate that the decreased neuroinflammation could relieve the reactive astrogliosis and improve the gamma oscillations.

A β load decreased by tUS

The total A β levels (A β 42 and A β 40) in cortical areas and the hippocampus were reduced after two weeks of tUS, compared to the Tg/Stim- group. The decrease in insoluble A β 42 in the Tg/Stim+ group was significant in the cortex but not in the hippocampus, whereas soluble A β 42 increased slightly but significantly compared to the Tg/Stim- group. Thus, in terms of A β level, tUS showed both therapeutic and potentially harmful effects simultaneously. The relative toxicity of soluble and insoluble A β is controversial. Insoluble A β fibrils aggregate from A β monomers and oligomers [40], and they can accumulate to form amyloid plaques, known to be pathological hallmarks in AD. The aggregation of insoluble fibrils causes neuroinflammation, which leads to neurite damage and decreases A β clearance [41, 42]. The fibrillar plaques are also causally related to progressive neuritic abnormalities in amyloid precursor protein transgenic mice [43, 44]. Indeed, our histological analysis showed reduced number of A β plaques in the hippocampus and decreased length and endpoints of microglial processes in the Tg/Stim+ group, implying the activation of microglia [23, 45].

According to our computational simulation of the affected regions by tUS stimulation, more than 60% of ultrasound wave pressure was transmitted through the mouse skull and reached the brain (Additional file 1: Fig. S1). Depending on the threshold value (-6 dB vs -12 dB) of the maximum simulatory acoustic pressure in the brain, 9% or 45% of brain volume was affected by tUS stimulation, respectively, even though the minimum acoustic pressure to stimulate the brain remains unclear. These results proved that the unfocused tUS affects a significant portion of the brain compared to focused tUS. Particularly, the region near the hippocampus appears to receive a stronger intensity of the ultrasound beams than PIL, resulting in more robust effects in histology.

The decrease in insoluble A β detected in this study may result in reduced neuroinflammation, or vice versa, in spite of the increase in soluble A β . However, amyloid oligomers are also soluble and can spread widely throughout the brain. The soluble oligomers can cause

hyper-phosphorylation of tau protein, which forms neurofibrillary tangles and leads to neuronal synaptic dysfunction in AD [46]. A β oligomers also induce the disruption of the neuritic cytoskeleton and accelerate cytotoxic effects [47]. Both fibrils and soluble A β have been found to induce cell death via different pathways: oligomers induce cell death via apoptosis, whereas amyloid fibrils lead to necrosis-like death [48]. Given that both insoluble and soluble A β are pathogenic via the sum of various mechanisms, such as neuroinflammation, synaptotoxicity and tau pathology, we may be able to suggest that the net effect of the tUS gamma entrainment might be therapeutic in spite of increased soluble fraction of A β . On the other hand, the timing of effects on A β may be different from previous research. The tUS stimulation might have a later therapeutic effect on the functionality of the brain than auditory or visual stimulation [23, 24], as in our consecutive analysis, the spontaneous gamma power showed significant improvement on day 14, but not on day 7. Direct comparison with the previous report on day 7 was not possible because we sampled the brain only on day 14. Nevertheless, since there is controversy on A β reduction as a therapeutic strategy, as was discussed recently on aducanumab [49], the importance of functional improvement may be more crucial as a direct indicator of therapeutic effect.

Functional improvement could be achieved by tUS

Recent studies have reported that the loss of EEG synchronization increases in AD patients and is correlated with cognitive dysfunction [20–22]. The gamma-band entrainment technique can improve cognitive function and memory performance [23, 24]. Because tUS at 40 Hz can increase the spontaneous gamma power, we investigated whether tUS could provide functional improvement in the 5 \times FAD mouse model. PLV can effectively reflect functional impairment of connectivity because it measures the temporal relationships of neural signals independent of their amplitude. Our results showed a decreasing trend in PLV in the sham treatment group (Tg/Stim-) over two weeks, while the direction of PLV changed in the treatment group (Tg/Stim+) from decrement (day 7 – baseline) to increment (day 14 – day 7), although there was no statistical significance. This suggests that the two weeks of ultrasound stimulation might have contributed to the recovery of PLV. We also analyzed the cross-frequency PAC to see how the phase of low-frequency oscillations modulates high-frequency power, especially the gamma band. The local processing could be fine-tuned or influenced by the modulation of gamma activity within particular areas by low-frequency oscillation. Recent studies revealed that the theta-phase high-gamma coupling correlates with working memory

by manipulating the ordering of information during the working memory process [39, 40]. Impairment of theta-gamma coupling followed by memory deficits has been reported by Goodman et al. in 2018 [41]. In our study, we observed reduction of theta-gamma PAC in Tg/Stim+ mice compared with WT at baseline. After 2 weeks of tUS stimulation, the theta-gamma coupling in Tg/Stim+ mice increased significantly in comparison to the baseline. Delta-gamma coupling is also considered as a biomarker for evaluating generalized EEG suppression and network activity [42]. Our results showed increased delta-gamma coupling in Tg/Stim+ mice on day 14 compared to baseline. Our results are consistent with a previous study by Yi Yuan et al., which showed that the PAC indices between the delta, theta, alpha, and gamma oscillations increased significantly with ultrasound stimulation [50], and thereby concluded that the ultrasound stimulation could be a powerful noninvasive method to interfere with the brain by modulating gamma oscillations in the rat hippocampus. Taken together, all of these results support that gamma-band entrainment by tUS stimulation at 40 Hz can normalize PLV and cross-frequency coupling, implying improved brain connectivity and information processing.

Ultrasound stimulation in AD treatment

Recently, several clinical studies have reported that ultrasound stimulation is a potential methodology to improve brain function and even cortical thickness in human AD patients. The promising results were replicated in independent groups over the last years, showing that transcranial pulse stimulation with focused ultrasound could improve neuropsychological scores and increase cortical thickness [51, 52]. In addition, low-intensity transcranial focused ultrasound (LI tFUS) has been reported with potential effects in AD treatment by Jeong et al. [53]. In their study, LI tFUS targeting the hippocampus has a beneficial impact on cerebral glucose metabolism and memory and improves cognitive function. Thus, a large body of preclinical and clinical evidence suggests that the blood–brain barrier (BBB) opening by FUS can be done safely [54, 55]. However, potential risks should be noted, including microbleeds, cellular vacuolation, ischemia due to vasoconstriction, cerebral edema, and direct cellular injury from physical forces, even at the typical low sound pressure [56]. Since most neuromodulation studies have been done without BBB opening and generated clear neurophysiological effects, non-BBB opening ultrasound ("focused" and "unfocused") might be a safer therapeutic option.

Conclusion

In this study, two-week tUS decreases total A β 42 and A β 40 levels, especially insoluble A β , in the brain cortex and hippocampus of 5 \times FAD mice. The reduction of A β plaque is comparable to the recent visual and auditory stimulation studies in AD mouse models. In addition, tUS stimulation increases spontaneous gamma power and PAC, indicative of functional improvement. In summary, tUS brain stimulation at 40 Hz can be a potential therapeutic modality by reducing A β load and improving brain connectivity. In future studies, the exact neurobiological mechanisms of these effects need to be investigated.

Abbreviations

AD: Alzheimer's disease; A β : Amyloid- β ; EEG: Electroencephalogram; WT: Wild type; tUS: Transcranial ultrasound stimulation; PSD: Power spectral density; PLV: Phase locking value; PAC: Phase-amplitude coupling; ELISA: Enzyme-linked immunosorbent assay; PBS: Phosphate-buffered saline; PIL: Pre- and infra limbic; RM ANOVA: Repeated measure analysis of variance; PV: Parvalbumin; FS-PV: Fast-spiking parvalbumin; NMDA: *N*-Methyl-*D*-aspartate.

Supplementary Information

The online version contains supplementary material available at <https://doi.org/10.1186/s40035-021-00274-x>.

Additional file 1: Fig. S1. Simulated acoustic pressure distribution in the brain during transcranial ultrasound simulation.

Acknowledgements

We thank Dr. Hwan Kim (GIST Central Research Facilities) for excellent technical assistance for the confocal microscopy.

Authors' contributions

MP, surgery, experiments, data analysis, manuscript writing; GMH, experiments, data analysis, manuscript writing; TN, designing experiments, preliminary investigation; EL, brain sample analysis; HJJ, designing experiments, data analysis; YC, designing experiments, data analysis; MHL, computer simulation and data interpretation; JYH, computer simulation, data interpretation; JGK, conceptualization, designing experiments, supervision, review & revision of the manuscript; TK, conceptualization, designing experiments, supervision, fund acquisition, review & revision of the manuscript. All authors read and approved the final manuscript.

Funding

This work was supported by the National Research Foundation of Korea (NRF) grant funded by the Korea government (Ministry of Science and ICT, 2016M3C7A1905475 and 2018R1A2B6006797 to JGK, 2017R1A5A1014708 and 2018 R1A2B6002804 to TK; Ministry of Education, 2015R1D1A1A01059119 to TK); 2021 Joint Research Project of Institutes of Science and Technology to TK; and KBRI basic research program through Korea Brain Research Institute funded by the Ministry of Science and ICT (21-BR-03-05) to JGK.

Availability of data and materials

The datasets used and/or analysed in the current study are available from the corresponding authors on reasonable request.

Declarations

Ethics approval and consent to participate

All works involving animals were approved by the ethics committee at Gwangju Institute of Science and Technology (GIST-2020-031) which is fulfilled

with Association for Assessment and Accreditation of Laboratory Animal Care International guidelines.

Consent for publication

All the authors have approved the manuscript.

Competing interests

The authors declare that they have no competing interests.

Author details

¹Department of Biomedical Science and Engineering, Gwangju Institute of Science and Technology, Gwangju 61005, Republic of Korea. ²Korea Brain Research Institute, Daegu 41062, Republic of Korea. ³Department of Information and Communication Engineering, Daegu Gyeongbuk Institute of Science and Technology, Daegu 42988, Republic of Korea.

Received: 21 July 2021 Accepted: 25 November 2021

Published online: 07 December 2021

References

1. Alzheimer's Association. 2013 Alzheimer's disease facts and figures. *Alzheimers Dement*. 2013;9(2):208–45.
2. Masters CL, Bateman R, Blennow K, Rowe CC, Sperling RA, Cummings JL. Alzheimer's disease. *Nat Rev Dis Primers*. 2015;1:1–18.
3. Chiba T, Yamada M, Sasabe J, Terashita K, Shimoda M, Matsuoka M, et al. Amyloid-beta causes memory impairment by disturbing the JAK2/STAT3 axis in hippocampal neurons. *Mol Psychiatry*. 2009;14:206–22.
4. Hardy J, Selkoe DJ. The amyloid hypothesis of Alzheimer's disease: progress and problems on the road to therapeutics. *Science*. 2002;297:353–6.
5. Zlokovic BV. Neurovascular pathways to neurodegeneration in Alzheimer's disease and other disorders. *Nat Rev Neurosci*. 2011;12:723–38.
6. Cserr HF, Harling-Berg CJ, Knopf PM. Drainage of brain extracellular fluid into blood and deep cervical lymph and its immunological significance. *Brain Pathol*. 1992;2:269–76.
7. Weller RO, Subash M, Preston SD, Mazanti I, Carare RO. Perivascular drainage of amyloid-beta peptides from the brain and its failure in cerebral amyloid angiopathy and Alzheimer's disease. *Brain Pathol*. 2008;18:253–66.
8. Mehta D, Jackson R, Paul G, Shi J, Sabbagh M. Why do trials for Alzheimer's disease drugs keep failing? A discontinued drug perspective for 2010–2015. *Expert Opin Investig Drugs*. 2017;26:735–9.
9. Cummings J, Lee G, Ritter A, Sabbagh M, Zhong K. Alzheimer's disease drug development pipeline: 2020. *Alzheimers Dement (N Y)*. 2020;6:e12050.
10. Abbott A, Dolgin E. Leading Alzheimer's theory survives drug failure. *Nature*. 2016;540:15–6.
11. Kaiser J, Lutzenberger W. Induced gamma-band activity and human brain function. *Neuroscientist*. 2003;9:475–84.
12. Colgin LL, Moser EI. Gamma oscillations in the hippocampus. *Physiology (Bethesda)*. 2010;25:319–29.
13. Traub RD, Whittington MA, Stanford IM, Jefferys JG. A mechanism for generation of long-range synchronous fast oscillations in the cortex. *Nature*. 1996;383:621–4.
14. Carlén M, Meletis K, Siegle JH, Cardin JA, Futai K, Vierling-Claassen D, et al. A critical role for NMDA receptors in parvalbumin interneurons for gamma rhythm induction and behavior. *Mol Psychiatry*. 2012;17:537–48.
15. Sohail VS, Zhang F, Yizhar O, Deisseroth K. Parvalbumin neurons and gamma rhythms enhance cortical circuit performance. *Nature*. 2009;459:698–702.
16. Palop JJ, Chin J, Roberson ED, Wang J, Thwin MT, Bien-Ly N, et al. Aberrant excitatory neuronal activity and compensatory remodeling of inhibitory hippocampal circuits in mouse models of Alzheimer's disease. *Neuron*. 2007;55:697–711.
17. Verret L, Mann EO, Hang GB, Barth AMI, Cobos I, Ho K, et al. Inhibitory interneuron deficit links altered network activity and cognitive dysfunction in Alzheimer model. *Cell*. 2012;149:708–21.
18. Gillespie AK, Jones EA, Lin YH, Karlsson MP, Kay K, Yoon SY, et al. Apolipoprotein E4 causes age-dependent disruption of slow gamma oscillations during hippocampal sharp-wave ripples. *Neuron*. 2016;90:740–51.

19. Mably AJ, Colgin LL. Gamma oscillations in cognitive disorders. *Curr Opin Neurobiol.* 2018;52:182–7.
20. Stam CJ, van Cappellen van Walsum AM, Pijnenburg YAL, Berendse HW, de Munck JC, Scheltens P, et al. Generalized synchronization of MEG recordings in Alzheimer's Disease: evidence for involvement of the gamma band. *J Clin Neurophysiol.* 2002;19:562–74.
21. Koenig T, Prichep L, Dierks T, Hubl D, Wahlund LO, John ER, et al. Decreased EEG synchronization in Alzheimer's disease and mild cognitive impairment. *Neurobiol Aging.* 2005;26:165–71.
22. Stam CJ, van der Made Y, Pijnenburg YAL, Scheltens P. EEG synchronization in mild cognitive impairment and Alzheimer's disease. *Acta Neurol Scand.* 2003;108:90–6.
23. Iaccarino HF, Singer AC, Martorell AJ, Rudenko A, Gao F, Gillingham TZ, et al. Gamma frequency entrainment attenuates amyloid load and modifies microglia. *Nature.* 2016;540:230–5.
24. Martorell AJ, Paulson AL, Suk HJ, Abdurrob F, Drummond GT, Guan W, et al. Multi-sensory gamma stimulation ameliorates Alzheimer's-associated pathology and improves cognition. *Cell.* 2019;177:256–271.e22.
25. Eguchi K, Shindo T, Ito K, Ogata T, Kurosawa R, Kagaya Y, et al. Whole-brain low-intensity pulsed ultrasound therapy markedly improves cognitive dysfunctions in mouse models of dementia—crucial roles of endothelial nitric oxide synthase. *Brain Stimul.* 2018;11:959–73.
26. Huang X, Lin Z, Wang K, Liu X, Zhou W, Meng L, et al. Transcranial low-intensity pulsed ultrasound modulates structural and functional synaptic plasticity in rat hippocampus. *IEEE Trans Ultrason Ferroelectr Freq Control.* 2019;66:930–8.
27. Lee Y, Choi Y, Park EJ, Kwon S, Kim H, Lee JY, et al. Improvement of glymphatic-lymphatic drainage of beta-amyloid by focused ultrasound in Alzheimer's disease model. *Sci Rep.* 2020;10:16144.
28. Bobola MS, Chen L, Ezeokeke CK, Olmstead TA, Nguyen C, Sahota A, et al. Transcranial focused ultrasound, pulsed at 40 Hz, activates microglia acutely and reduces A β load chronically, as demonstrated in vivo. *Brain Stimul.* 2020;13:1014–23.
29. Oakley H, Cole SL, Logan S, Maus E, Shao P, Craft J, et al. Intraneuronal beta-amyloid aggregates, neurodegeneration, and neuron loss in transgenic mice with five familial Alzheimer's disease mutations: potential factors in amyloid plaque formation. *J Neurosci.* 2006;26:10129–40.
30. Franklin K, Paxinos G. The mouse brain in stereotaxic coordinates, compact. 3rd ed. San Diego: Academic Press; 2008.
31. Jäkel L, De Kort AM, Klijn CJM, Schreuder FHBM, Verbeek MM. Prevalence of cerebral amyloid angiopathy: a systematic review and meta-analysis. *Alzheimers Dement.* 2021. <https://doi.org/10.1002/alz.12366>.
32. Ye PP, Brown JR, Pauly KB. Frequency dependence of ultrasound neurostimulation in the mouse brain. *Ultrasound Med Biol.* 2016;42:1512–30.
33. Riis T, Kubanek J. Effective ultrasonic stimulation in human peripheral nervous system. *IEEE Trans Biomed Eng.* 2021. <https://doi.org/10.1109/TBME.2021.3085170>.
34. Kwon JS, O'Donnell BF, Wallenstein GV, Greene RW, Hirayasu Y, Nestor PG, et al. Gamma frequency-range abnormalities to auditory stimulation in schizophrenia. *Arch Gen Psychiatry.* 1999;56:1001–5.
35. Adaikkan C, Middleton SJ, Marco A, Pao PC, Mathys H, Kim DNW, et al. Gamma entrainment binds higher-order brain regions and offers neuroprotection. *Neuron.* 2019;102:929–943.e8.
36. Jones RS, Bühl EH. Basket-like interneurons in layer II of the entorhinal cortex exhibit a powerful NMDA-mediated synaptic excitation. *Neurosci Lett.* 1993;149:35–9.
37. Browne TC, McQuillan K, McManus RM, O'Reilly JA, Mills KHG, Lynch MA. IFN- γ Production by amyloid β -specific Th1 cells promotes microglial activation and increases plaque burden in a mouse model of Alzheimer's disease. *J Immunol.* 2013;190:2241–51.
38. Ta TT, Dikmen HO, Schilling S, Chausse B, Lewen A, Hollnagel JO, et al. Priming of microglia with IFN- γ slows neuronal gamma oscillations *in situ*. *Proc Natl Acad Sci U S A.* 2019;116:4637–42.
39. Jo S, Yarishkin O, Hwang YJ, Chun YE, Park M, Woo DH, et al. GABA from reactive astrocytes impairs memory in mouse models of Alzheimer's disease. *Nat Med.* 2014;20:886–96.
40. Brown MR, Radford SE, Hewitt EW. Modulation of β -amyloid fibril formation in Alzheimer's disease by microglia and infection. *Front Mol Neurosci.* 2020;13:609073.
41. Bamberger ME, Harris ME, McDonald DR, Husemann J, Landreth GE. A cell surface receptor complex for fibrillar beta-amyloid mediates microglial activation. *J Neurosci.* 2003;23:2665–74.
42. Heneka MT, Golenbock DT, Latz E. Innate immunity in Alzheimer's disease. *Nat Immunol.* 2015;16:229–36.
43. Yankner BA, Lu T. Amyloid beta-protein toxicity and the pathogenesis of Alzheimer disease. *J Biol Chem.* 2009;284:4755–9.
44. Meyer-Luehmann M, Spies-Jones TL, Prada C, Garcia-Alloza M, de Calignon A, Rozkalne A, et al. Rapid appearance and local toxicity of amyloid-beta plaques in a mouse model of Alzheimer's disease. *Nature.* 2008;451:720–4.
45. Morrison H, Young K, Qureshi M, Rowe RK, Lifshitz J. Quantitative microglia analyses reveal diverse morphologic responses in the rat cortex after diffuse brain injury. *Sci Rep.* 2017;7:13211.
46. Chen GF, Xu TH, Yan Y, Zhou YR, Jiang Y, Melcher K, et al. Amyloid beta: structure, biology and structure-based therapeutic development. *Acta Pharmacol Sin.* 2017;38:1205–35.
47. Jin M, Shepardson N, Yang T, Chen G, Walsh D, Selkoe DJ. Soluble amyloid beta-protein dimers isolated from Alzheimer cortex directly induce Tau hyperphosphorylation and neuritic degeneration. *Proc Natl Acad Sci U S A.* 2011;108:5819–24.
48. Gharibyan AL, Zamotin V, Yanamandra K, Moskaleva OS, Margulis BA, Kostanyan IA, et al. Lysozyme amyloid oligomers and fibrils induce cellular death via different apoptotic/necrotic pathways. *J Mol Biol.* 2007;365:1337–49.
49. Liu KY, Howard R. Can we learn lessons from the FDA's approval of aducanumab? *Nat Rev Neurol.* 2021;17:715–22.
50. Yuan Y, Yan J, Ma Z, Li X. Effect of noninvasive focused ultrasound stimulation on gamma oscillations in rat hippocampus. *NeuroReport.* 2016;27:508–15.
51. Popescu T, Pernet C, Beisteiner R. Transcranial ultrasound pulse stimulation reduces cortical atrophy in Alzheimer's patients: a follow-up study. *Alzheimers Dement (NY).* 2021;7:e12121.
52. Beisteiner R, Matt E, Fan C, Baldysiak H, Schönfeld M, Philipp Novak T, et al. Transcranial pulse stimulation with ultrasound in Alzheimer's disease—a new navigated focal brain therapy. *Adv Sci (Weinh).* 2020;7:1902583.
53. Jeong H, Im JJ, Park JS, Na SH, Lee W, Yoo SS, et al. A pilot clinical study of low-intensity transcranial focused ultrasound in Alzheimer's disease. *Ultrasonography.* 2021;40:512–9.
54. Meng Y, Hynynen K, Lipsman N. Applications of focused ultrasound in the brain: from thermoablation to drug delivery. *Nat Rev Neurol.* 2021;17:7–22.
55. Park SH, Baik K, Jeon S, Chang WS, Ye BS, Chang JW. Extensive frontal focused ultrasound mediated blood-brain barrier opening for the treatment of Alzheimer's disease: a proof-of-concept study. *Transl Neurodegener.* 2021;10(1):44.
56. Beisteiner R, Lozano AM. Transcranial ultrasound innovations ready for broad clinical application. *Adv Sci (Weinh).* 2020;7(23):2002026.

Ready to submit your research? Choose BMC and benefit from:

- fast, convenient online submission
- thorough peer review by experienced researchers in your field
- rapid publication on acceptance
- support for research data, including large and complex data types
- gold Open Access which fosters wider collaboration and increased citations
- maximum visibility for your research: over 100M website views per year

At BMC, research is always in progress.

Learn more biomedcentral.com/submissions

